Early Detection of Corrosion Damage in Reinforced Concrete Using GPR Array Imaging Method

Weixia Cheng, Hai-Han Sun, Kang Hai Tan, and Zheng Fan

***Abstract*—Corrosion of reinforcing bars constitutes a significant factor contributing to cracking and spalling in reinforced concrete (RC) structures. To prolong the service life of RC structures, it is crucial to develop a robust non-destructive inspection system for early-stage corrosion damage assessment. Although ground-penetrating radar (GPR) has proven its effectiveness in detecting severe corrosion damage, identifying early-stage corrosion with conventional GPR methods with single-input-single-output (SISO) configuration is challenging due to their limited sensitivity to subtle changes in the properties of the reinforcing bar and the surrounding environment. To address this challenge, this study introduces a method that employs a GPR array to increase sensitivity in detecting early-stage corrosion. The method uses a linear multiple-input-multiple-output (MIMO) GPR array to reconstruct images of the reinforcing bars during the corrosion process. The reconstructed images are highly sensitive to corrosion-induced rusts and cracks that exhibit different dielectric permittivity and conductivity compared to the concrete. By analyzing the differences in these images from those of bars in a healthy state using the structural similarity (SSIM) index, the progression of corrosion can be precisely identified. The effectiveness of this method has been validated through numerical simulations and experimental corrosion monitoring tests. Compared to conventional SISO GPR configurations, the MIMO array offers a broader perspective in sensing corrosion products surrounding the reinforcing bars, thereby improving sensitivity and robustness in detecting early-stage corrosion.**

***Index Terms*—Early detection of corrosion, ground-penetrating radar, multiple-input-multiple-output (MIMO) array, reinforced concrete, structural similarity (SSIM)**

I. Introduction

CORROSION of reinforcing bars stands as a pivotal determinant in the degradation of reinforced concrete (RC) structures. The buildup of expansive corrosion products causes tensile stresses within the concrete, leading to the formation of cracks and spalling of the concrete cover. In addition, the reduction in the cross-sectional area of reinforcing bars compromises the bonding strength between reinforcing bars and concrete, diminishing the overall loading capacity of RC structures. To extend the lifespan of RC structures, it is imperative to establish a robust non-destructive inspection technique to evaluate corrosion damage at its early stages.

This work was supported by the Ministry of Education of Singapore Tier-1 grant (RG69/22). (*Corresponding authors: Zheng Fan; Hai-Han Sun)*

W. Cheng and Z. Fan are with the School of Mechanical and Aerospace Engineering, Nanyang Technological University, Singapore, 639798 (e-mail: wxcheng@ntu.edu.sg, zfan@ntu.edu.sg).

H. H. Sun is with Department of Electrical and Computer Engineering, University of Wisconsin-Madison, 1415 Engineering Dr, Madison, WI 53706, US (e-mail: haihan.sun@wisc.edu).

K. H. Tan is with the School of Civil and Environmental Engineer, Nanyang Technological University, Singapore, 639798 (e-mail: ckhtan@ntu.edu.sg).

Various non-destructive inspection methods have been investigated to assess corrosion damage in concrete, including electrochemical methods [1]–[3], X-ray computed tomography (X-ray CT) [4]–[6], ultrasonic methods [7]–[10], and electromagnetic methods [11]–[13]. Traditionally, electrochemical methods involve half-cell potential and polarization resistance measurements [1]–[3]. The corrosion potential serves to assess the likelihood of corrosion in testing areas [1]–[3], [14], while polarization resistance aids in calculating the corrosion current density, thus estimating the mass loss of reinforcing bars [15]–[18]. However, these measurements are destructive, which require drilling holes to connect the device with reinforcing bars [1]. X-ray CT technology has been utilized to monitor the progression of corrosion by analyzing X-ray attenuation [4]–[6], [19]. Nonetheless, the trade-off between image resolution and specimen size restricts the ability to detect small cracks and rust in large concrete samples [19]. Ultrasonic methods have been explored for detecting corrosion-induced cracks based on the change in acoustic impedance [7], [8]. However, these methods lack sensitivity to changes in reinforcing bars caused by corrosion.

Ground penetrating radar (GPR), which uses electromagnetic waves to inspect subsurface structures, has been extensively studied for corrosion assessment in concrete [11], [12], [20]–[24]. The behavior of electromagnetic waves propagation in a material depends on its dielectric permittivity and conductivity [13]. Corrosion, as a form of chemical deterioration, arises from the ingress of water, carbonation, and chloride. It generates corrosion products and cracks with various dielectric permittivity and conductivity compared to concrete, influencing the propagation of electromagnetic waves [13]. Analyses of reflections from reinforcing bars throughout the corrosion process have been conducted using a single-input-single-output (SISO) configuration [25]–[30]. Some studies indicate that corrosion results in a decrease in amplitude and an increase in travel time of reflections of the reinforcing bar [25], [26], [30], whereas, Lai *et al.* [29], [31], [32] demonstrated that the reflection of corroded reinforcing bars exhibit an increased amplitude and a decreased travel time. The discrepancies in phenomena related to corrosion in different literature can be attributed to the different experimental setups employed in the accelerated corrosion process. Besides the corrosion products, corrosion-induced cracks also significantly affect the amplitude of reflections [32], [33]. The previous studies primarily used a pair of antennas with polarization that is parallel to the orientation of the reinforcing bar to evaluate the corrosion, whereas dual-polarized antennas with polarizations that are parallel and perpendicular to the bar orientation have also been

employed to detect corrosion damage in concrete, based on polarimetric decomposition [34], [35].

In the abovementioned studies, GPR has proven effective in detecting corrosion damage in RC structures. However, identifying early-stage corrosion, defined as the phase where only rust forms, remains challenging. This is partly due to the limited data obtained from a standard configuration involving only a single pair of transmit and receive antennas, referred to as a single-input-single-output (SISO) configuration. Such a setup restricts the range of perspectives and angles for the electromagnetic waves to interact with the reinforcing bar. Moreover, the impact of temperature variations on GPR signals has been neglected in prior studies, potentially masking the identification of subtle changes induced by the initial thin layer of rust.

Multiple-input-multiple-output (MIMO) antenna arrays can concurrently transmit and receive multiple signals of different traveling paths, capturing more geometric information for subsurface targets compared to SISO configurations [36]. MIMO arrays have been widely used to reconstruct subsurface objects [36]–[38]. Recent developments include the successful utilization of MIMO arrays to accurately estimate the diameter of healthy reinforcing bars in concrete [39]. Corrosion of reinforcing bars introduces corrosion products, causes cracks, and alters the shape of the bars. In comparison to the SISO configuration, the MIMO array can provide more information about these subtle changes around the bars under corrosion due to its broader coverage. This capability holds significant potential for assessing the early-stage corrosion of reinforcing bars.

In this paper, we introduce a method to detect early-stage corrosion in RC samples using MIMO GPR array imaging. The method involves utilizing a linear antenna array to collect full-matrix data that capture the comprehensive reflected signals from the reinforcing bar in the concrete in the corrosion process. This full-matrix data is then processed using a diffraction stacking algorithm to reconstruct the image of the reinforcing bar undergoing corrosion. Since corrosion results in the reduction in the cross-sectional areas of reinforcing bars and the formation of rust and cracks with different permittivity, these physical changes influence the reconstructed images. However, temperature fluctuations also affect these images by altering the dielectric permittivity and conductivity of the materials involved, leading to measurement uncertainty. To address this issue, the Optimal Baseline Selection (OBS) method is utilized to mitigate the influence of temperature. Subsequently, the structural similarity (SSIM) algorithm is employed to quantify the changes in reconstructed images and correlate them with early-stage corrosion progression. Numerical simulations and experimental monitoring tests have been conducted to evaluate the effectiveness of the proposed method. The method shows high sensitivity in detecting corrosion damage in concrete, particularly in identifying rust accumulation and crack propagation in the early stages of corrosion.

II. Testing Approach

A. Numerical Model

Numerical models are developed first to simulate the MIMO GPR array method to access the image variation with different levels of corrosion damage using open-source software gprMax [40], [41]. As shown in Fig. 1, a reinforcing bar with a diameter of 16 mm is located at a cover depth of 30 mm in a concrete slab. The spatial discretization is 0.05 mm in the x- and z- directions. A perfectly matched layer (PML) is implemented around the concrete model to prevent reflections from the boundary. The material properties of components in the RC model are detailed in Table I [42], [43]. A linear array consisting of 6 y-polarized hertzian dipoles spaced 10 mm apart is utilized to acquire the full matrix data. The excitation signal for the source is a 6 GHz Ricker pulse.

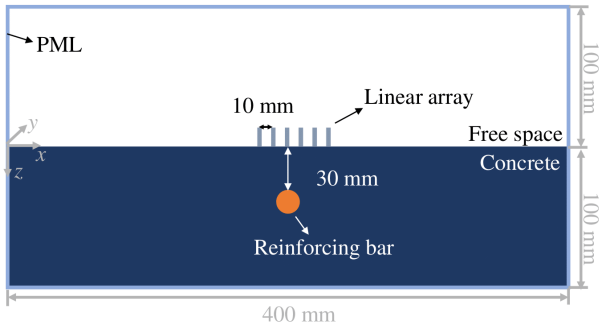

Fig. 1. Schematic of the simulation model in gprMax2D software [40], [41].

TABLE I
Material Properties Used in the RC Model [42], [43].

Materials	Rust	Air (crack)	Concrete	Reinforcing bar
Relative permittivity	10	1	6	1
Electrical conductivity (S/m)	0.00001	0	0.01	∞

To explore the impact of corrosion damage on reconstructed images of the reinforcing bar, 18 scenarios are created with varying levels of rust thicknesses and crack sizes to simulate different levels of corrosion damage, as shown in Fig. 2. The symbols RT and VL represent the maximum rust thickness and the maximum vertical length of the crack, respectively, indicating the corrosion levels of the reinforcing bar. These simulated scenarios of corrosion damage were referenced from previous research on the subject [8], [44], [45]. Since there is an interface layer (air) between a reinforcing bar and concrete [44], in the corrosion-free scenario (C#1), a simulated air layer of 0.1 mm around the reinforcing bar is modeled. Given that corrosion tends to initiate predominantly on the upper surface of reinforcing bars due to their proximity to the concrete surface [45], we simulated two scenarios, C#2 and C#3, with rust thicknesses RT of 0.05 mm and 0.1 mm, respectively, occupying the upper air layer of the reinforcing bar. Rust is shown in red color in the figures. This phase is characterized by the free expansion of rust accumulation. Subsequently, the expansion of rust introduces tensile stresses surpassing the tensile strength of mortar, leading to the emergence of micro-cracks in scenario C#4 (in green color). As

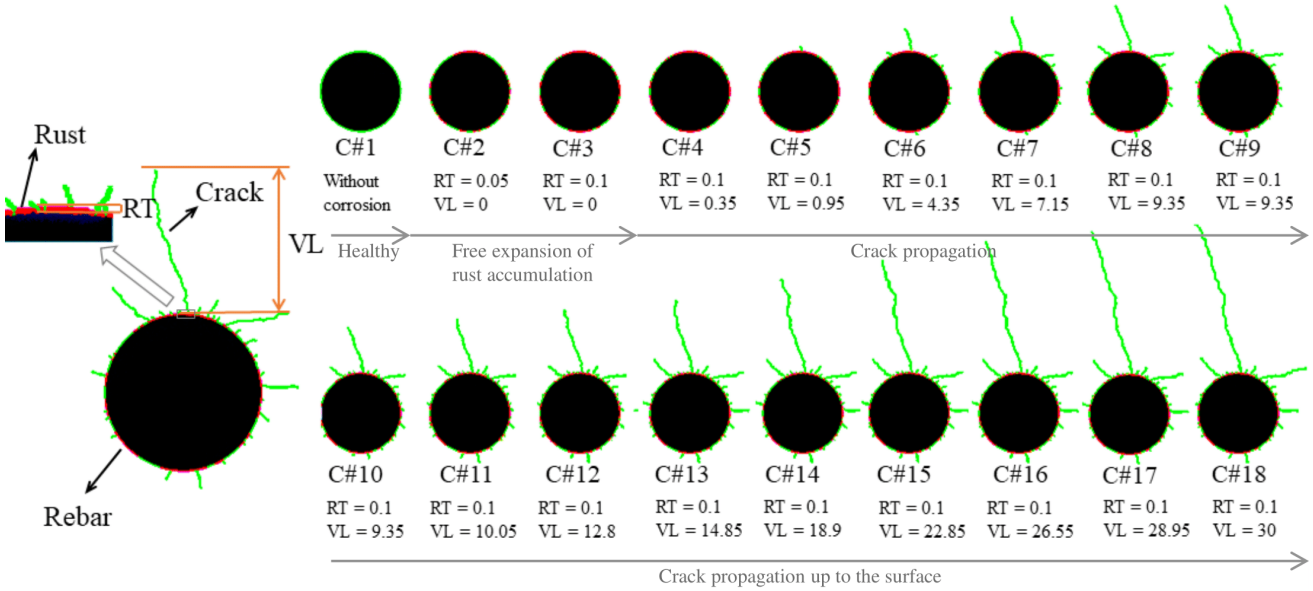

Fig. 2. Simulated models of a reinforcing bar with varying levels of rust thicknesses and crack sizes. Rust and cracks are shown in red and green colors, respectively.

the corrosion progresses, cracks expand, as shown in scenarios C#5 to C#18, and ultimately approach the concrete surface in scenario C#18.

B. Experimental Setup

1) Accelerated Corrosion: A reinforced concrete slab measuring 600 mm × 300 mm × 100 mm was cast and sufficiently cured for 28 days before the initiation of corrosion testing. The slab was reinforced with two reinforcing bars with diameters of 16 mm, which were positioned 30 mm below the surface. To simulate a realistic distribution of chlorides, the specimen was first submerged in a 5% sodium chloride solution for 5 days. After this, it was removed from the water bath and stored in the laboratory for 5 months to attain a relatively stable moisture content within the concrete.

An accelerated corrosion process of the reinforcing bar was achieved by subjecting the sample to direct current under dry conditions. As shown in Fig. 3, a reinforcing bar was connected to the positive terminal of a DC power source as the anode for corrosion, while another bar was connected to the negative terminal as the cathode. The experiment involved an initial phase with a constant current density of 100 $\mu A/cm^2$ for the first 227 hours, followed by an increase to 200 $\mu A/cm^2$ until the 395th hour when a fine crack appeared on the surface of the concrete. At this point, the corrosion test was concluded.

2) Corrosion Monitoring using GPR Array: Fig. 3 illustrates the experimental setup used for the corrosion monitoring test. The GPR array used in this experiment has 6 antenna elements with a spacing of 10 mm. The antenna is a self-designed Vivaldi antenna [46] operating from 1.3 GHz to 9.0 GHz. Each antenna was connected to an individual channel of a 6-port vector network analyzer (Keysight VNA P5022A). To achieve a balanced compromise between the detection ability and sensitivity to the reinforcing bar, an ultra-wide

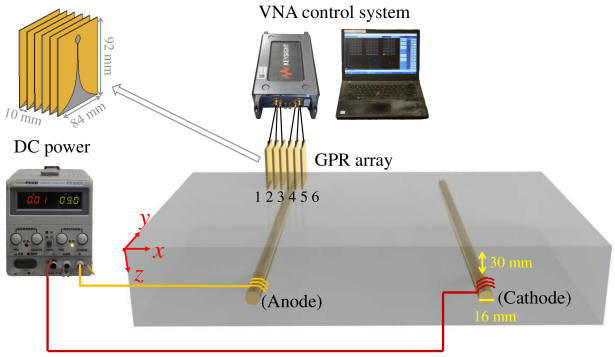

Fig. 3. Experimental configuration of the corrosion monitoring system.

frequency band ranging from 2.9 GHz to 9 GHz was chosen, and a total of 801 sample points were recorded. Each antenna served as both the transmitter and receiver, so for each MIMO GPR measurement, 6×6 full matrix data are collected. The MIMO GPR array measurements were conducted periodically to monitor the accelerated corrosion process. To capture early-stage corrosion information, the data was recorded every hour for the initial 11 hours, followed by longer intervals of 2, 4, 10, and 24 hours, respectively.

C. GPR Array Imaging for Early-Stage Corrosion Monitoring

Upon acquiring the full matrix data corresponding to one scenario, the diffraction stacking algorithm was utilized to reconstruct the reinforcing bar. This algorithm is to reconstruct the intensity I at each pixel position (x, z) in the image by summing the signals based on the time of flight [47]. It is expressed as:

$$I(x,z) = \left| \sum_{i=1}^{N} \sum_{j=1}^{N} CS_{ij}\left(\frac{l_i + l_j}{v}\right) \right| = \left| \sum_{i=1}^{N} \sum_{j=1}^{N} CS_{ij}\left(\frac{\sqrt{(x_i - x)^2 + z^2} + \sqrt{(x_j - x)^2 + z^2}}{v}\right) \right|. \quad (1)$$

Here N denotes the number of antennas, which is 6 in this study; CS_{ij} represents the complex signal that is transmitted by antenna i and received by antenna j, involving both amplitude and phase information; The distances from the transmitting antenna to the pixel (x, z) and from the pixel (x, z) to the receiving antenna are denoted as l_i and l_j, respectively; x_i and x_j denote the x-coordinate of the transmitting antenna i and the receiving antenna j, respectively; The velocity of electromagnetic waves propagating in concrete is denoted as v and is determined by $v = c/\sqrt{\varepsilon_r}$, where c stands for the speed of light and ε_r is the relative dielectric permittivity of the concrete.In this study, A-scan signal was collected from the surface of the concrete. The velocity of wave propagation in concrete was determined based on the time difference between surface reflection and bottom reflection from concrete, as well as the sample thickness $v = \frac{2\times h}{T_2 - T_1}$, where h represents the thickness of concrete sample, and T_1 and T_2 denote the arrival times of surface reflection and bottom reflection, respectively.

As corrosion can lead to a decrease in the cross-sectional area of the reinforcing bar, along with the formation of rust and cracks, the dielectric permittivity and conductivity of the corroded reinforcing bar undergo significant changes compared to its healthy state. Consequently, the reconstructed image of reinforcing bars would be affected. The structural similarity (SSIM) algorithm is utilized to assess the changes in the reconstructed images in the progression of corrosion. This algorithm quantifies the similarity between the reference reconstructed image I_0 and reconstructed image I_n during the corrosion process. The similarity measurement considers three comparisons between the two images: luminance $l(I_0, I_n)$, contrast $c(I_0, I_n)$, and structure $s(I_0, I_n)$ [48], which are defined as:

$$l(I_0, I_n) = \frac{2\mu_{I_0}\mu_{I_n} + C_1}{\mu_{I_0}^2 + \mu_{I_n}^2 + C_1}. \quad (2)$$

$$c(I_0, I_n) = \frac{2\sigma_{I_0}\sigma_{I_n} + C_2}{\sigma_{I_0}^2 + \sigma_{I_n}^2 + C_2}. \quad (3)$$

$$s(I_0, I_n) = \frac{\sigma_{I_0 I_n} + C_3}{\sigma_{I_0}\sigma_{I_n} + C_3}. \quad (4)$$

In the equations, μ_{I_0} and μ_{I_n} denote the mean values of images I_0 and I_n, and σ_{I_0} and σ_{I_n} represent the variances of images I_0 and I_n; The term $\sigma_{I_0 I_n}$ denotes the covariance between images I_0 and I_n; The constants C_1, C_2, and C_3 stabilize these computations, especially when the denominators become small [48].

The structural similarity index $SSIM(I_0, I_n)$ is defined as a multiplication of these three comparisons. A simplified expression is presented as [48]:

$$SSIM(I_0, I_n) = \frac{(2\mu_{I_0}\mu_{I_n} + C_1)(2\sigma_{I_0 I_n} + C_2)}{(\mu_{I_0}^2 + \mu_{I_n}^2 + C_1)(\sigma_{I_0}^2 + \sigma_{I_n}^2 + C_2)}. \quad (5)$$

A lower SSIM index indicates a greater difference between images.

An example of a reconstructed image of a reinforcing bar is presented in Fig. 4.

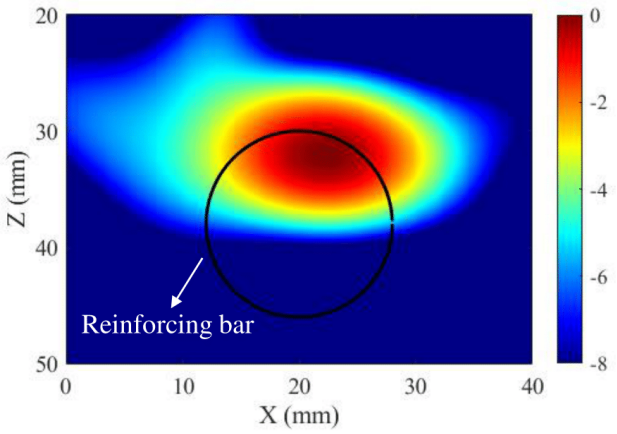

Fig. 4. Diffraction stacking migration imaging result for a reinforcing bar with a diameter of 16 mm.

D. Optimal Baseline Selection Method for Temperature Compensation

GPR array measurements were carried out in the laboratory under the operation of an air conditioner. The ambient temperature in the laboratory is measured using a thermocouple, with fluctuations of 1°C. It should be noted that temperature fluctuations affect the propagation of electromagnetic waves, as they would lead to changes in the dielectric permittivity and conductivity of materials [49]. In Fig. 5, the black curve illustrates the SSIM index of reconstructed images of a healthy reinforcing bar over a temperature range of 23.2°C to 24.4°C before temperature compensation, and the standard deviation is measured as 0.011. Notably, during the early stage of corrosion, the thickness of corrosion-induced rust is generally smaller than 0.2 mm [44], which is significantly less than the wavelength employed in this study (approximately 20 mm). Consequently, the impact on the SSIM index of the reconstructed image due to rust formation in the initial stage is minimal. For instance, in simulation scenario C#2, the reduction in the SSIM index is only 5e-4. Given these observations, it becomes imperative to address and mitigate the impact of temperature fluctuations on the monitoring results.

In this study, the Optimal Baseline Selection (OBS) method is employed for temperature compensation [50]. This method utilizes a set of M baseline signals acquired at different temperatures as reference data. The objective is to identify the baseline signal $x_m(t)$ that optimally aligns with the current testing signal $x(t)$ recorded at temperature T. The maximum residual amplitude method is employed as a metric to evaluate the similarity between the current testing signal and baseline signals [51]:

$$m_{mr} = \arg\min_{m} \{\max |x(t;T) - x_m(t;T_m)|\}, \quad (6)$$

where m_{mr} is the baseline signal that exhibits the most optimal alignment with the current testing signal. In this experiment, we established a comprehensive baseline dataset comprising a total of 1136 sets of full matrix data recorded at temperatures ranging from 21°C to 26°C. The range covers the temperature range in our laboratory in Singapore, where the air conditioner operates during the day and remains inactive at night.

The red curve in Fig. 5 shows the SSIM index of the reconstructed image after temperature compensation. It can be seen that the application of the OBS method effectively mitigates the impact of temperature fluctuations on the GPR array imaging results. This is highlighted by a notable reduction in the standard deviation of the SSIM index by two orders of magnitude. The standard deviation after the temperature compensation is 1.6e-4.

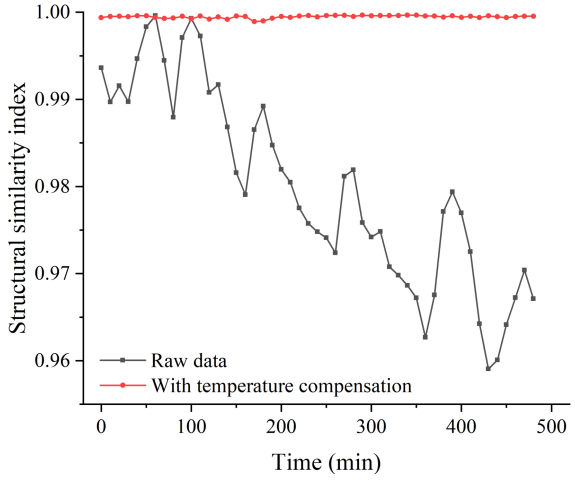

Fig. 5. The SSIM index of reconstructed images with temperatures ranging from 23.2°C to 24.3°C before and after temperature compensation.

III. Results Analysis

A. Results from Numerical Simulation

Fig. 6 presents the SSIM index of reconstructed images of a reinforcing bar subjected to different degrees of simulated corrosion damage. There is a noticeable decrease in the SSIM index from scenarios C#1 to C#3, indicating increased dissimilarity between the reconstructed images. This trend stems from the effect of rust filling the air layer, which consequently alters the shape of the reconstructed images. From C#3 to C#5 and C#8 to C#10, the appearance of micro-cracks induces negligible changes in the SSIM index due to their small dimensions. From C#5 to C#8 and C#10 to C#14, a notable decrease in the SSIM index is observed with the substantial expansion of internal cracks. However, from C#14 to C#17, as cracks approach the surface of the concrete, the SSIM index undergoes a relatively small fluctuation. This phenomenon is attributed to the reduced impact of reflections from vertical internal cracks on the reconstructed areas surrounding the reinforcing bar. In contrast, a significant decrease in the SSIM index for scenario C#18 can be observed, which is primarily caused by the expansion of horizontal cracks. The simulated results demonstrate the effectiveness of the proposed MIMO GPR array imaging method in detecting corrosion damage, including the identification of thin layers of rust and crack propagation.

B. Results from Experimental Monitoring

1) Monitoring Initial Stage of Corrosion: The accelerated corrosion process described in Section II-B1 was monitored for a duration of 395 hours until the appearance of a fine crack on the concrete surface. To provide a comprehensive analysis of the early stage of corrosion, defined as the phase where only rust forms, monitoring results for the SSIM index of reconstructed images of the reinforcing bar from the initial 13 hours of corrosion are shown in Fig. 7.

It can be observed that there was a decrease in the SSIM index within the first 5 hours of corrosion. From the 6th hour to the 7th hour, the variation in the SSIM index was minimal, followed by a significant decrease. This pattern aligned with results observed in simulated scenarios from C#1 to C#8. Consequently, the decrease in the initial 5 hours of corrosion should be attributed to the accumulation of rust, filling the air layer with various dielectric permittivity, thereby affecting the reconstructed images. Subsequently, the micro-cracks appeared and continued to grow, leading to more pronounced reflections and a significant decrease in the SSIM index after the 7th hour. The corrosion monitoring results in the initial stages validate that the MIMO array imaging method effectively detects thin layers of rust and micro-cracks.

2) Monitoring Crack Propagation: Fig. 8 presents the monitoring results for the SSIM index of reconstructed images for the entire corrosion process, which spans a duration of 395 hours until the appearance of a surface-breaking crack. A significant decrease was observed after the 7th hour. These decreases aligned with results observed in simulated scenarios from C#5 to C#8 and C#10 to C#14, indicating their association with the enlargement of cracks. Beyond the 117th hour, the SSIM index exhibited relatively moderate changes, consistent with results observed in simulated scenarios from C#14 to C#18. This phase can be attributed to expanded cracks approaching the concrete surface, mitigating their impact on the reconstructed area around the reinforcing bar. The relatively significant decrease during this phase, such as at the 395th hour, may be due to expanded cracks in other directions, as exemplified in the simulated scenario C#18.

The entire corrosion monitoring results obtained from the MIMO array imaging method align well with numerical simulations, demonstrating its effectiveness in detecting corrosion damage in concrete, including the identification of rust accumulation and crack propagation. The results show the applicability of the proposed method in monitoring corrosion damage throughout the entire corrosion process.

3) Comparison of Monitoring Results between Conventional SISO Configuration and MIMO Array Imaging: The performance of the MIMO GPR array imaging method in identifying early corrosion damage, specifically rust accumulation, is compared with that of the conventional SISO GPR

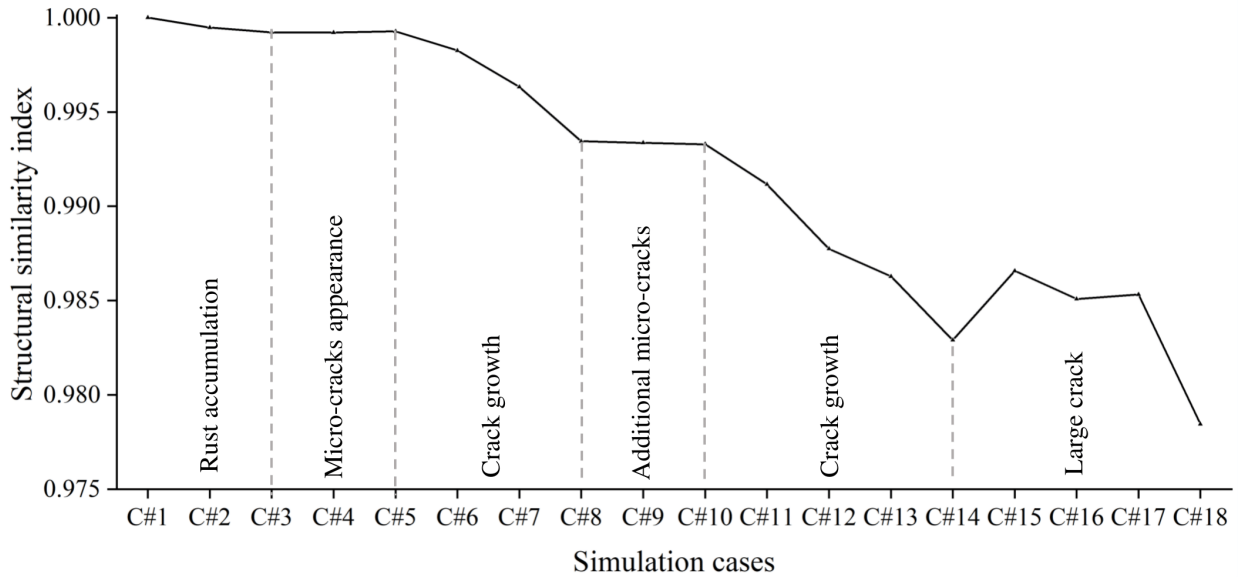

Fig. 6. The SSIM index of reconstructed images of the reinforcing bar with various simulated corrosion damage.

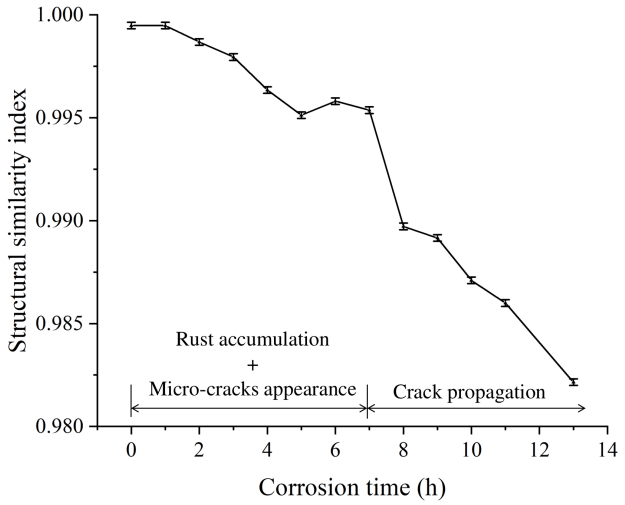

Fig. 7. Monitoring results over a 13-hour duration of accelerated corrosion using the MIMO GPR array. The SSIM index of reconstructed images has a standard deviation of 1.6e-4.

configuration using the experimental results. Referring to the antenna positions in Fig. 3, the SISO configurations include the following cases: transmission from antenna 1 and reception by antenna 5 with a spacing of 40 mm (S1R5); transmission from antenna 1 and reception by antenna 6 with a spacing of 50 mm (S1R6); and transmission from antenna 3 and reception by antenna 3 (S3R3).

Fig. 9 presents the monitoring results of the normalized maximum amplitude of reinforcing bar reflections in various SISO configurations. The error bar after temperature compensation is also presented. In the S1R5 configuration, subtle amplitude variation was observed within the initial 3 hours of corrosion, which falls below the threshold of measurement errors. The subtle amplitude changes in this time frame may result from the limited angle of observation provided by the SISO setup, which cannot fully capture the thin rust distribution. The increase in amplitude at the 4th hour, surpassing the measurement error, could be attributed to the accumulation of rust. This accumulation introduced a multiple interface, leading to stronger reflections. Furthermore, the significant amplitude increased at the 7th hour may be due to reflections from expanding cracks, aligning with the SSIM index monitoring results shown in Section III-B1. However, in comparison, the amplitudes of reinforcing bar reflections obtained from the S1R6 and S3R3 configurations exhibit fluctuations during the first 13-hour corrosion period. The fluctuations can be attributed to rust not being situated on specific propagation paths associated with these SISO configurations. The fluctuations within the range of measurement errors make these configuration incapable of detecting early-stage corrosion-induced damage. The results obtained from various SISO configurations shown in Fig. 9 demonstrate that the performance of the SISO configuration in detecting early-stage corrosion is significantly affected by the positioning of the antenna pairs.

Comparing the monitoring results obtained from MIMO array shown in Fig. 7 and SISO configurations shown in Fig. 9, it is evident that the SSIM index from MIMO array imaging shows a noticeable decrease starting from one hour onwards, whereas the change in amplitude acquired from the SISO configuration in the best case (S1R5) only slightly surpasses the measurement error after four hours of corrosion. It demonstrates that the MIMO array imaging method is more effective and sensitive in detecting the initial thin layer of rust. This superiority of the MIMO array imaging method can be attributed to the MIMO array's capability to capture comprehensive information from a wider range of angles at which electromagnetic waves interact with the corroded reinforcing bar. In contrast, the SISO configuration can only

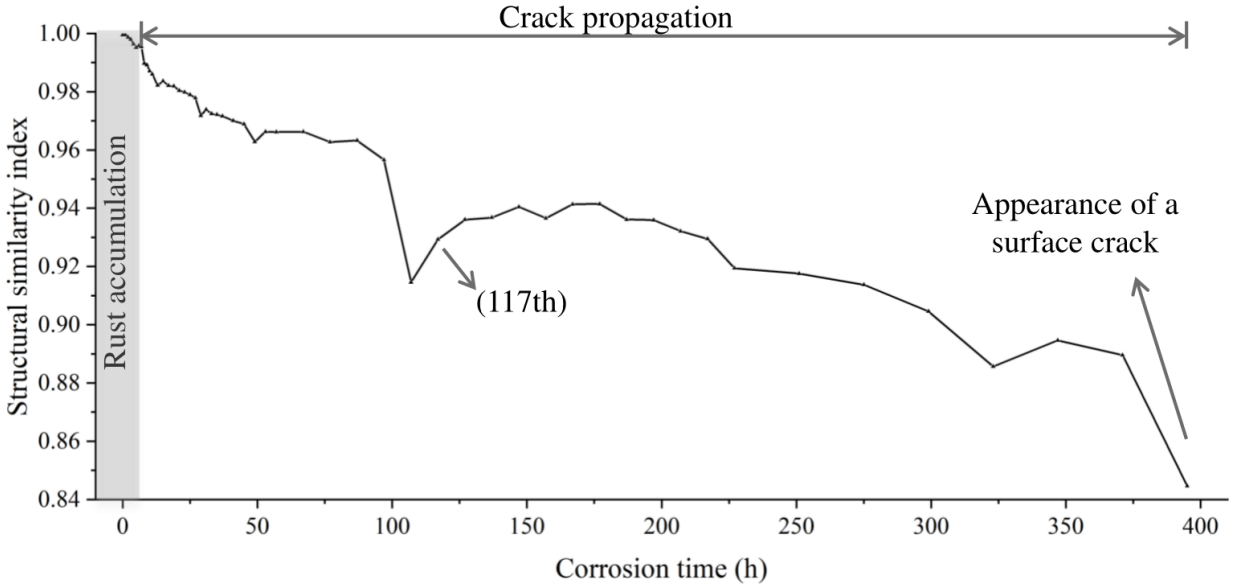

Fig. 8. Monitoring results over a 395-hour duration of accelerated corrosion using the MIMO GPR array. The SSIM index of reconstructed images has a standard deviation of 1.6e-4.

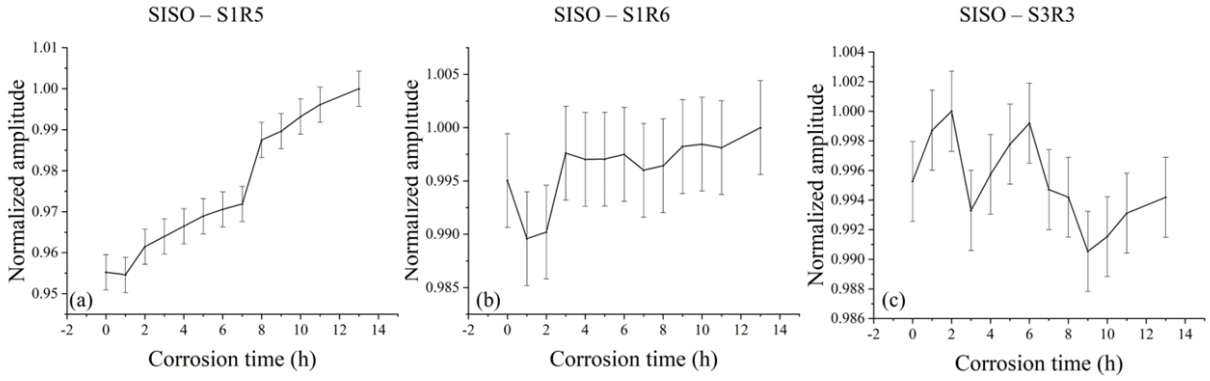

Fig. 9. Monitoring results for the normalized maximum amplitude of reinforcing bar reflections obtained from SISO configurations over a 13-hour corrosion duration: (a) emitted at antenna 1 received at antenna 5 with a standard deviation of 4.3e-3, (b) emitted at antenna 1 received at antenna 6 with a standard deviation of 4.4e-3, (c) emitted at antenna 3 received at antenna 3 with a standard deviation of 2.7e-3.

acquire limited information from a specific angle. Additionally, the positioning of the antenna pair in the SISO configuration significantly affects the effectiveness of corrosion damage detection, introducing uncertainty and unreliability in the identification of corrosion progression.

IV. Conclusion

In this paper, we present a method for assessing the corrosion of reinforcing bars in RC structures using MIMO GPR array imaging. In our method, the diffraction stacking algorithm is employed to reconstruct reinforcing bars in concrete using the full-matrix data obtained by the MIMO antenna array. The reconstructed image is highly sensitive to rust and cracks in the corrosion process. The SSIM index between the reconstructed images of the reinforcing bar at different corrosion levels and the image of the healthy bar is used to evaluate corrosion damage. Numerical simulation with various levels of corrosion damage and experimental monitoring measurements have been carried out to validate the performance of the method. The experimental monitoring results align closely with the simulated ones, and both demonstrate that the SSIM index shows a discernible decrease as rust accumulates and a significant decrease as cracks expand.

The advantage of the MIMO GPR array imaging method in detecting early-stage corrosion is further confirmed through a comparison with the results obtained using the conventional amplitude method with the SISO configuration. The measurement results show that the SSIM index notably decreases after just one hour of corrosion with the MIMO configuration, while the amplitude changes of the reinforcing bar reflection only slightly exceed the measurement error after four hours of corrosion in the best SISO case. Furthermore, the ability to detect early corrosion damage using the SISO configuration is greatly influenced by the antenna position. The comparison highlights the advantage of the proposed MIMO array imaging method in providing high sensitivity and robustness in detecting early-

stage corrosion.

In addition to the capability of assessing the development of corrosion in an individual point of reinforcing bar, this method also has the potential to serve as a portable inspection tool for evaluating the overall corrosion condition of structures through scanning tests. However, it is worth noting that, for measurement calibration, it is necessary to fix measurement points and collect baseline data within the typical environmental temperature range. Nevertheless, compared to the widely adopted SISO configuration, our MIMO array imaging method has greater potential for assessing the subtle changes in material properties of concrete in the early stages of corrosion.

REFERENCES

[1] C. ASTM, "Standard test method for half-cell potentials of uncoated reinforcing steel in concrete," 1999.

[2] B. Elsener, C. Andrade, J. Gulikers, R. Polder, and M. Raupach, "Half-cell potential measurements—potential mapping on reinforced concrete structures," Mater. Struct., vol. 36, no. 7, pp. 461–471, 2003.

[3] S. Feliu, J. Gonzalez, S. Feliu, and C. Andrade, "Relationship between conductivity of concrete and corrosion of reinforcing bars," Br. Corros. J., vol. 24, no. 3, pp. 195–198, 1989.

[4] A. Michel, B. J. Pease, M. R. Geiker, H. Stang, and J. F. Olesen, "Monitoring reinforcement corrosion and corrosion-induced cracking using non-destructive x-ray attenuation measurements," Cem Concr Res, vol. 41, no. 11, pp. 1085–1094, 2011.

[5] P.-A. Itty, M. Serdar, C. Meral, D. Parkinson, A. A. MacDowell, D. Bjegovi´c, and P. J. Monteiro, "In situ 3d monitoring of corrosion on carbon steel and ferritic stainless steel embedded in cement paste," Corros. Sci., vol. 83, pp. 409–418, 2014.

[6] M. Beck, J. Goebbels, A. Burkert, B. Isecke, and R. B¨aßler, "Monitoring of corrosion processes in chloride contaminated mortar by electrochemical measurements and x-ray tomography," Mater. Corros., vol. 61, no. 6, pp. 475–479, 2010.

[7] W. Cheng, H.-H. Sun, L. S. Wan, Z. Fan, and K. H. Tan, "Corrosion damage detection in reinforced concrete using rayleigh wave-based method," Cem Concr Compos, vol. 143, p. 105253, 2023.

[8] W. Cheng, Z. Fan, and K. H. Tan, "Characterisation of corrosion-induced crack in concrete using ultrasonic diffuse coda wave," Ultrasonics, vol. 128, p. 106883, 2023.

[9] E. Larose, T. Planes, V. Rossetto, and L. Margerin, "Locating a small change in a multiple scattering environment," Appl. Phys. Lett., vol. 96, no. 20, pp. 1–4, 2010.

[10] W.-J. Song, J. S. Popovics, J. C. Aldrin, and S. P. Shah, "Measurement of surface wave transmission coefficient across surface-breaking cracks and notches in concrete," J. Acoust. Soc. Am., vol. 113, no. 2, pp. 717–725, 2003.

[11] A. Robert, "Dielectric permittivity of concrete between 50 Mhz and 1 GHz and GPR measurements for building materials evaluation," J Appl Geophy, vol. 40, no. 1-3, pp. 89–94, 1998.

[12] J. Hugenschmidt and R. Loser, "Detection of chlorides and moisture in concrete structures with ground penetrating radar," Mater Struct, vol. 41, no. 4, pp. 785–792, 2008.

[13] Z. Sbarta¨ı, S. Laurens, J.-P. Balayssac, G. Arliguie, and G. Ballivy, "Ability of the direct wave of radar ground-coupled antenna for ndt of concrete structures," NDT E Int., vol. 39, no. 5, pp. 400–407, 2006.

[14] G. Glass, C. Page, and N. Short, "Factors affecting the corrosion rate of steel in carbonated mortars," Corros. Sci., vol. 32, no. 12, pp. 1283–1294, 1991.

[15] C. Andrade and J. Gonz´alez, "Quantitative measurements of corrosion rate of reinforcing steels embedded in concrete using polarization resistance measurements," Mater. Corros., vol. 29, no. 8, pp. 515–519, 1978.

[16] K. C. Clear, "Measuring rate of corrosion of steel in field concrete structures," Transp. Res. Rec., no. 1211, 1989.

[17] C. Andrade, M. C. Alonso, and J. A. Gonzalez, "An initial effort to use the corrosion rate measurements for estimating rebar durability," Corrosion rates of steel in concrete, ASTM STP, vol. 1065, pp. 29–37, 1990.

[18] C. Newton and J. Sykes, "A galvanostatic pulse technique for investigation of steel corrosion in concrete," Corros. Sci., vol. 28, no. 11, pp. 1051–1074, 1988.

[19] S. Lim, M. Akiyama, D. M. Frangopol, and H. Jiang, "Experimental investigation of the spatial variability of the steel weight loss and corrosion cracking of reinforced concrete members: novel x-ray and digital image processing techniques," Struct. Infrastruct. Eng., vol. 13, no. 1, pp. 118–134, 2017.

[20] K. Dinh, N. Gucunski, and T. Zayed, "Automated visualization of concrete bridge deck condition from GPR data," NDT E Int., vol. 102, no. November 2018, pp. 120–128, 2019.

[21] K. Dinh, N. Gucunski, J. Kim, and T. H. Duong, "NDT and E International Method for attenuation assessment of GPR data from concrete bridge decks," NDT E Int., vol. 92, no. August, pp. 50–58, 2017.

[22] K. Dinh, T. Zayed, F. Romero, and A. Tarussov, "Method for Analyzing Time-Series GPR Data of Concrete Bridge Decks," J. Bridge Eng., vol. 20, no. 6, p. 04014086, 2015.

[23] M. Abouhamad, T. Dawood, A. Jabri, M. Alsharqawi, and T. Zayed, "Corrosiveness mapping of bridge decks using image-based analysis of GPR data," Autom. Constr., vol. 80, pp. 104–117, 2017.

[24] A. Tarussov, M. Vandry, and A. De La Haza, "Condition assessment of concrete structures using a new analysis method: Ground-penetrating radar computer-assisted visual interpretation," Constr Build Mater., vol. 38, pp. 1246–1254, 2013.

[25] V. Sossa, V. P´erez-Gracia, R. Gonz´alez-Drigo, and M. A. Rasol, "Lab non destructive test to analyze the effect of corrosion on ground penetrating radar scans," Remote Sens., vol. 11, no. 23, p. 2814, 2019.

[26] A. Zaki, M. A. Megat Johari, W. M. A. Wan Hussin, and Y. Jusman, "Experimental assessment of rebar corrosion in concrete slab using ground penetrating radar (gpr)," Int. J. Corros., vol. 2018, 2018.

[27] S. Hong, W. L. Lai, and R. Helmerich, "Experimental monitoring of chloride-induced reinforcement corrosion and chloride contamination in concrete with ground-penetrating radar," Struct. Infrastruct. Eng., vol. 11, no. 1, pp. 15–26, 2015.

[28] S. Hong, W. W.-l. Lai, G. Wilsch, R. Helmerich, R. Helmerich, T. G¨unther, and H. Wiggenhauser, "Periodic mapping of reinforcement corrosion in intrusive chloride contaminated concrete with GPR," Constr. Build. Mater., vol. 66, pp. 671–684, 2014.

[29] W.-L. Lai, T. Kind, M. Stoppel, and H. Wiggenhauser, "Measurement of accelerated steel corrosion in concrete using ground-penetrating radar and a modified half-cell potential method," J. Infrastruct. Syst., vol. 19, no. 2, pp. 205–220, 2013.

[30] S. S. Hubbard, J. Zhang, P. J. Monteiro, J. E. Peterson, and Y. Rubin, "Experimental detection of reinforcing bar corrosion using nondestructive geophysical techniques," Materials Journal, vol. 100, no. 6, pp. 501–510, 2003.

[31] W. L. Lai, T. Kind, and H. Wiggenhauser, "Using ground penetrating radar and time–frequency analysis to characterize construction materials," NDT E Int., vol. 44, no. 1, pp. 111–120, 2011.

[32] W. L. Lai, T. Kind, and H. Wiggenhauser, "Detection of accelerated reinforcement corrosion in concrete by ground penetrating radar," in Proceedings of the XIII Internarional Conference on Ground Penetrating Radar. IEEE, 2010, pp. 1–5.

[33] P. T. Wong, W. W. Lai, J. F. Sham, and C.-s. Poon, "Hybrid nondestructive evaluation methods for characterizing chloride-induced corrosion in concrete," NDT E Int., vol. 107, p. 102123, 2019.

[34] H.-H. Sun, W. Cheng, and Z. Fan, "Diameter estimation of cylindrical metal bar using wideband dual-polarized ground-penetrating radar," IEEE Trans. Instrum. Meas., vol. 72, pp. 1–14, 2023.

[35] H. Liu, J. Zhong, F. Ding, X. Meng, C. Liu, and J. Cui, "Detection of early-stage rebar corrosion using a polarimetric ground penetrating radar system," Constr Build Mater., vol. 317, p. 125768, 2022.

[36] A. Martinez-Vazquez and J. Fortuny-Guasch, "Uwb mimo radar arrays for small area surveillance applications," in The Second European Conference on Antennas and Propagation, EuCAP 2007. IET, 2007, pp. 1–6.

[37] T. Savelyev, X. Zhuge, A. Yarovoy, L. Ligthart, and B. Levitas, "Comparison of uwb sar and mimo-based short-range imaging radars," in 2009 European Radar Conference (EuRAD). IEEE, 2009, pp. 109–112.

[38] A. Srivastav, P. Nguyen, M. McConnell, K. A. Loparo, and S. Mandal, "A highly digital multiantenna ground-penetrating radar (gpr) system," IEEE Trans. Instrum. Meas., vol. 69, no. 10, pp. 7422–7436, 2020.

[39] W. Cheng, H.-H. Sun, K. H. Tan, and Z. Fan, "Estimating the diameter of reinforcing bars using an ultra-wideband mimo gpr array," Constr. Build. Mater., vol. 365, p. 129924, 2023.

[40] C. Warren, A. Giannopoulos, and I. Giannakis, "gprMax: Open source software to simulate electromagnetic wave propagation for Ground Penetrating Radar," Comput. Phys. Commun., vol. 209, pp. 163–170, 2016.
[41] C. Warren, A. Giannopoulos, A. Gray, I. Giannakis, A. Patterson, L. Wetter, and A. Hamrah, "A CUDA-based GPU engine for gprMax: Open source FDTD electromagnetic simulation software," Comput. Phys. Commun., vol. 237, pp. 208–218, 2019.
[42] C. Amer-Yahia and T. Majidzadeh, "Inspection of insulated concrete form walls with ground penetrating radar," Constr Build Mater., vol. 26, no. 1, pp. 448–458, 2012.
[43] N. J. Cassidy and T. M. Millington, "The application of finite-difference time-domain modelling for the assessment of gpr in magnetically lossy materials," J Appl Geophy, vol. 67, no. 4, pp. 296–308, 2009.
[44] S. Car´e, Q. T. Nguyen, V. L'Hostis, and Y. Berthaud, "Mechanical properties of the rust layer induced by impressed current method in reinforced mortar," Cem. Concr. Res., vol. 38, no. 8-9, pp. 1079–1091, 2008.
[45] Y. Zhao, B. Hu, J. Yu, and W. Jin, "Non-uniform distribution of rust layer around steel bar in concrete," Corros. Sci., vol. 53, no. 12, pp. 4300–4308, 2011.
[46] P. J. Gibson, "The vivaldi aerial," in 1979 9th European Microwave Conference. IEEE, 1979, pp. 101–105.
[47] E. M. Johansson and J. E. Mast, "Three-dimensional ground-penetrating radar imaging using synthetic aperture time-domain focusing," Advanced Microwave and Millimeter-Wave Detectors, vol. 2275, no. September 1994, pp. 205–214, 1994.
[48] Z. Wang, A. C. Bovik, H. R. Sheikh, and E. P. Simoncelli, "Image quality assessment: from error visibility to structural similarity," IEEE Trans Image Process, vol. 13, no. 4, pp. 600–612, 2004.
[49] J. M. Wraith and D. Or, "Temperature effects on soil bulk dielectric permittivity measured by time domain reflectometry: Experimental evidence and hypothesis development," Water Resour. Res., vol. 35, no. 2, pp. 361–369, 1999.
[50] A. J. Croxford, J. Moll, P. D. Wilcox, and J. E. Michaels, "Efficient temperature compensation strategies for guided wave structural health monitoring," Ultrasonics, vol. 50, no. 4-5, pp. 517–528, 2010.
[51] T. Clarke, F. Simonetti, and P. Cawley, "Guided wave health monitoring of complex structures by sparse array systems: Influence of temperature changes on performance," J. Sound Vib., vol. 329, no. 12, pp. 2306–2322, 2010.

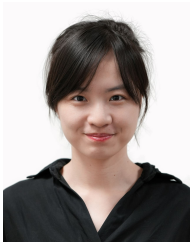

Weixia Cheng obtained her bachelor's degree in civil engineering from Central South university in 2014, master's degree in structural engineering from Tianjin university in 2017, and the Ph.D degree in mechanics engineering from Nanyang Technological University, Singapore, in 2023. She is currently a research fellow at Nanyang Technological University, Singapore. Her research topic is the corrosion damage detection in reinforced concrete using non-destructive testing methods including ultrasonic wave and ground-penetrating radar.

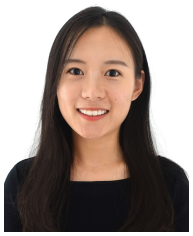

Hai-Han Sun received her bachelor's degree in electronic information engineering from Beijing University of Posts and Telecommunications, Beijing, China, in 2015, and the Ph. D. degree in engineering from the University of Technology Sydney, Australia, in 2019. From 2019 to 2023, she was a Research Fellow at Nanyang Technological University, Singapore. She is currently an assistant professor in the Department of Electrical and Computer Engineering at the University of Wisconsin-Madison. Her research interests include ground-penetrating radar, base station antenna, electromagnetic sensing, and non-destructive testing methodologies.

Kang Hai Tan obtained his PhD degree at The University of Manchester. He is currently a professor in the School of Civil and Environmental Engineering, Nanyang Technological University, Singapore. His research interests include fire effects on steel, concrete and composite steel structures, strut and tie modelling of RC structures, beam-column joint behaviour, progressive collapse resistance testing and nonlinear finite element analysis, and development of sustainable concrete. He is a Specialist Professional Engineer in Protective Security.

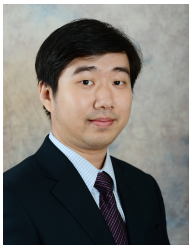

Zheng Fan obtained his PhD degree at Imperial College London, specialized in Non-Destructive Evaluation (NDE). He is currently an associate professor in the school of Mechanical and Aerospace Engineering at Nanyang Technological University in Singapore, leading a research team to develop novel techniques for metal and composite inspection, structural health monitoring and material characterization, by integrating physics and modeling techniques with the development of rapidly exploitable technologies.